water may also be in equilibrium with locally derived plant CO_2, as HCO_3^- is in soil water.

Other evidence also supports a pedogenic origin for the Trench 14 carbonates. The morphology (*2*) and petrography of the carbonates and silica fillings are consistent with a soil origin, as is micromorphological, clay mineralogical, trace element (*18*), and isotope tracer (*19*) evidence. Oxygen isotopes from the silica cements indicate that the temperatures of formation were ~15°C, consistent with that in a pedogenic environment (*2*).

REFERENCES AND NOTES

1. P. S. Justus and N. K. Stablein, *Geotimes* **34**, 14 (1989); papers presented at the DOE/NRC meeting on the calcite and opaline silica peer review, 25 to 27 May 1987, Las Vegas, NV; D. T. Vaniman, D. L. Bish, S. Chipera, *Los Alamos Natl. Lab. Rep. LA-11289-MS (UC-70)* (1988).
2. E. M. Taylor, *U.S. Geol. Surv. Bull.*, in press.
3. J. Quade, T. E. Cerling, J. R. Bowman, *Geol. Soc. Am. Bull.* **101**, 464 (1989).
4. W. G. Spaulding, *U.S. Geol. Surv. Prof. Pap.* **1329** (1985). Spaulding mainly sampled middens from all around the adjacent Nevada Test Site and Amargosa Desert, within ~100 km of Trench 14, and from the Sheep Range near Las Vegas.
5. L. H. Gile, F. F. Peterson, R. B. Grossman, *Soil Sci.* **101**, 347 (1966). Weak Stage I refers to pedogenic carbonate only as coatings on clast undersides.
6. J. Quade, *Quat. Res.* **26**, 340 (1986); E. M. Taylor, thesis, University of Colorado, Boulder (1986); S. G. Wells, L. D. McFadden, J. C. Dohrenwend *Quat. Res.* 27, 130 (1987). Soil carbonate development is dependent on time and other factors, such as parent material, dust flux, and so forth. However, weak stage I morphology is observed to be associated with surfaces younger than late Pleistocene, irrespective of parent material. Carbonate coatings of our samples were discontinuous patches on clast undersides and were ≤1 mm in thickness. Clasts were occasionally encrusted with older cements, and these were avoided. The patterns displayed by stable C isotopes in these soils (*3*) indicate that there has been negligible detrital contamination or inheritance from dissolution of parent material. As such, these dates represent a composite age of all the layers of carbonate present. Because of the very young ages we obtained, it is unlikely that any pre-Holocene component to the carbonate is present.
7. T. E. Cerling, J. Quade, Y. Wang, J. R. Bowman, *Nature* **341**, 138 (1989). Complete isotopic equilibrium between C species is obtained before the precipitation of soil carbonate, and this accounts for 10 to 11 per mil of the enrichment. Diffusion effects on soil CO_2 account for about 4.4 per mil further enrichment in the carbonates. Parent material has no influence on the outcome (*3*). All stable isotope analyses on carbonates are reported relative to PDB (Pee Dee Belemnite) using standard notation, where $\delta^{13}C(PDB)$ or $\delta^{18}O(PDB) = ([(R_{sample}/R_{standard}) - 1] \times 1000)$ and $R = (^{13}C/^{12}C_{sample})/(^{13}C/^{12}C_{standard})$ or $^{18}O/^{16}O_{sample}/^{18}O/^{16}O_{standard}$, respectively. The isotopic composition of water is reported relative to SMOW (standard mean ocean water).
8. CAM plants, which include cactus and most yucca, are present at lower elevations but don't exceed 10% of the biomass at any site. They average −18 per mil in $\delta^{13}C$.
9. We observed that the $\delta^{13}C$ (PDB) and the $\delta^{18}O$ (PDB) of carbonates appear to be constant below about 40-cm depth in modern soils at this general elevation (*3*). Above 40 cm, mixing with the atmospheric CO_2 causes progressive enrichment up to the soil surface. All the Trench 14 samples come from 0.9 to 3.4 m below the surface, and display no systematic trends with depth. All our modern soil carbonates that we used to fingerprint isotopically each of the vegetation zones come from 0.5 to 2.2 m depth.
10. I. J. Winograd, B. J. Szabo, T. B. Coplen, A. C. Riggs, *Science* **242**, 1275 (1988).
11. H. C. Claassen, *Chem. Geol. (Isot. Geosci. Sect.)* **58**, 311 (1986); L. Benson and H. Klieforth, in *Aspects of Climate Variability in the Pacific and Western Americas*, D. H. Peterson, Ed. (*Monogr. 55*, American Geophysical Union, Washington, DC, 1989), pp. 41–59.
12. J. N. Rosholt *et al.*, *U.S. Geol. Surv. Open-File Rep. 85-540* (1985). At least three episodes of faulting and subsequent fracture filling are evident from cross-cutting relations in the south wall of Trench 14 (*2*). The age of the last event is currently assessed at no older than 300,000 years ago and is likely around 150,000 years ago. This estimate is based on the estimated age of the Stage IV petrocalcic horizon [see (*5*) for this terminology] cut by the youngest fissures and the presence in one fissure of a basaltic ash thought to be 150,000 years old. The two earlier faulting episodes do not cut the Stage IV carbonates or deposits dated by U-trend methods at about 450,000 years ago. This method, however, remains experimental. The few published U-series dates on the veins are problematic because they contain excess ^{232}Th, and therefore do not exhibit closed-system behavior. More dates, particularly by the U-series and ^{14}C methods, are clearly warranted.
13. R. L. Hay, R. E. Pexton, T. T. Teague, T. K. Kyser, *Geol. Soc. Am. Bull.* 97, 1488 (1986).
14. L. V. Benson and P. W. McKinley, *U.S. Geol. Surv. Open-File Rep. 85-484* (1985).
15. To calculate the maximum possible temperatures of carbonate formation, we used −11.5 per mil (SMOW) for ground water (interglacial water) and the most depleted carbonates from Trench 14, −11.5 per mil (PDB). This gives a temperature of 15.4°C. Waters showing a typical glacial-age composition [−13.5 per mil (SMOW)] give a temperature of 7.3°C.
16. I. J. Winograd and W. Thordarson, *U.S. Geol. Survey Prof. Pap. 712-C* (1975).
17. P. D. Coplen and I. J. Winograd, in preparation.
18. D. T. Vaniman, D. L. Bish, S. Chipera, *Los Alamos Natl. Lab. Rep.* LA-11289-MS (UC-70) (1988).
19. D. R. Muhs, J. W. Whitney, R. R. Shroba, E. M. Taylor, C. A. Bush, *Proceedings of the International High-level Nuclear Waste Management Conference*, Las Vegas, NV, 8 to 12 April, (American Society of Civil Engineers, New York, 1990).

20. We thank M. Mifflin, I. Winograd, and L. Benson for their useful discussions and help, and R. J. Johnson for his logistical assistance. Analyses were performed at the University of Utah and Yale University. This work was supported primarily by the Nevada Nuclear Waste Project Office, and by National Science Foundation grant BNS-8703304.

25 June 1990; accepted 3 October 1990

The Kangmar Dome: A Metamorphic Core Complex in Southern Xizang (Tibet)

Z. Chen, Y. Liu, K. V. Hodges, B. C. Burchfiel, L. H. Royden, C. Deng

The Kangmar metamorphic-igneous complex is one of the most accessible examples of an enigmatic group of gneiss domes (the North Himalayan belt) that lies midway between the Greater Himalaya and the Indus-Tsangpo suture in southern Tibet. Structural analysis suggests that the domal structure formed as a consequence of extensional deformation, much like the Tertiary metamorphic core complexes in the North American Cordillera. Unlike its North American counterparts, the Kangmar dome developed in an entirely convergent tectonic setting. The documentation of metamorphic core complexes in the Himalayan orogen supports the emerging concept that extensional processes may play an important role in the evolution of compressional mountain belts.

Although the Himalayan orogen developed as a consequence of continent-continent collision between India and Eurasia during Eocene time and subsequently has accommodated continued convergence between these plates, recent studies of the geology of southern Tibet have revealed that extensional faults characteristic of divergent settings like the Basin and Range province of western North America are common at high structural levels in the Himalaya (*1–3*). These faults are interpreted as facilitating the lateral spreading of isostatically compensated, tectonically thickened lithosphere under the influence of gravity (*2, 4–6*).

The presence of extensional structures in southern Tibet raises an important question: how many features that we commonly think of as characteristic of divergent settings can develop in convergent settings? Some of the most striking extensional features of the Basin and Range province are gneiss domes referred to as metamorphic core complexes. Since their recognition as extensional phenomena (7), these complexes have been found in numerous extensional settings worldwide but never in convergent settings. A series of gneiss domes forms an east-west trending belt roughly halfway between the crest of the Himalayas and the Indus-Tsangpo suture [Fig. 1; the Lhagoi Kangri or North Himalayan belt (*8*)]. Some of the gross features of these domes suggest that

Z. Chen, Y. Liu, C. Deng, Chengdu Institute of Geology and Mineral Resources, Chengdu, People's Republic of China.
K. V. Hodges, B. C. Burchfiel, L. H. Royden, Department of Earth, Atmospheric, and Planetary Sciences, Massachusetts Institute of Technology, Cambridge, MA 02139.

they may be metamorphic core complexes. In this report, we describe mesoscopic and microscopic deformational features of one of the North Himalayan gneiss domes located north of Kangmar (28°40′N; 89°40′E) in southern Tibet and show that the most prominent fabrics represent ductile extensional deformation after an earlier compressional event, similar to fabric relations observed near the top of the Greater Himalayan metamorphic sequence (*2, 8*).

The Kangmar dome occurs in the Tibetan Sedimentary Zone, a region dominated by shallow marine continental rocks of Ordovician to Permian age and marine rocks deposited on the passive margin of India from Triassic to Eocene(?) time (*9, 10*). The oldest structures in the Tibetan Sedimentary Zone, south-vergent thrust and fold nappes of Late Cretaceous to Paleocene age, apparently formed during obduction. Eocene to Miocene(?) structures related to collision include shallowly dipping, south-vergent thrust faults and steeply dipping, north-vergent backthrusts (*11, 12*). Precambrian and younger(?) metasedimentary and metaigneous units of the Greater Himalayan Sequence occur south of the Tibetan Sedimentary Zone (*9*). These rocks were metamorphosed to amphibolite facies at temperatures greater than 800 K during Himalayan orogenesis (*13*); in many areas, substantial volumes of late Oligocene(?) to Miocene leucogranite melt were produced (*14*). The contact between the Greater Himalayan Sequence and the Tibetan Zone is a system of north-dipping, low-angle normal faults of Miocene age (*15*) that may have helped to accommodate gravitational collapse of topography created by collisional thickening (*2*). Numerous other Miocene to Pliocene(?), east-west trending normal faults and related fold structures in Southern Tibet appear to have been related to this event as well. The youngest structures in the region are Pliocene(?) to Recent, north-south trending normal faults associated with east-west extension of the Tibetan Plateau (*16*).

The Kangmar dome consists of a core of Cambrian granitic gneiss mantled by metasedimentary and sedimentary rocks ranging in age from Paleozoic to Jurassic (Fig. 2). The contact between the orthogneiss and its cover has been described as intrusive (*17, 18*) or uncomformable (*8, 19*), but most researchers have attributed high-grade metamorphism and coeval deformation in the core of the gneiss dome to Tertiary compressional processes related to Himalayan orogenesis. The Kangmar dome is a north-south trending, doubly plunging anticline. Stratal dips near the northern terminus average 40° to 50°N, whereas those at the southern terminus are slightly less steep (30° to 40°S). As a consequence, outcrop patterns of units in the dome are somewhat asymmetric. Doming has resulted in the exposure of lithologic units ranging in age from Cambrian to Triassic.

The core of the dome consists of a mylonitic granite gneiss that has yielded a U-Pb zircon age of 562 ± 4 Ma (*20*). This augen gneiss is separated from its metasedimentary and sedimentary cover by zone of intense ductile shearing and subsequent brecciation. This contact is interpreted as a fault, and we

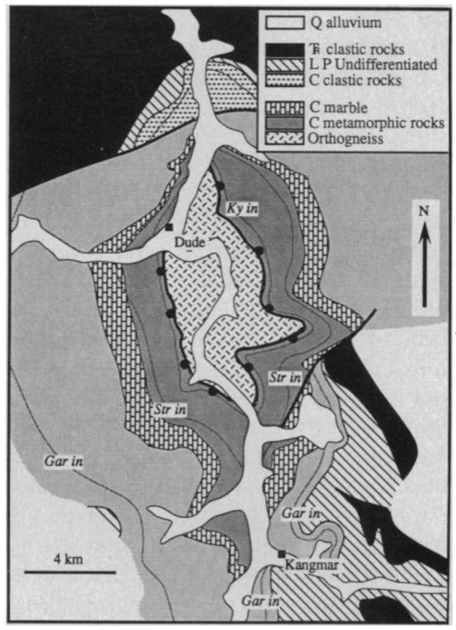

Fig. 2. Generalized geologic map of the Kangmar dome; Str in, staurolite isograd; Gar in, garnet isograd; Ky in, kyanite isograd; Q, Quarternary; L P, Lower Permian; C, Carboniferous; TR Triassic.

refer to it as the Kangmar detachment. Metasedimentary rocks above the detachment include pelitic schists, quartzites, and marbles (*8*). Low-grade marbles high in this section contain Carboniferous fossils of the *Orthotichia-Wilkingia* assemblage (*21*), but the ages of lower units above the detachment are only presumed to be Carboniferous on the basis of their lithologic similarity with fossiliferous units elsewhere in the region. Structurally higher lithologies include a weakly metamorphosed, mixed carbonate and clastic rock sequence assigned to the Permian system, overlain by unmetamorphosed sandstones and shales of Triassic age.

Thermobarometric studies of mineral assemblages in rocks just above the Kangmar detachment indicate that peak metamorphic conditions were 750 to 875 K and 725 to 850 MPa (*8, 22*). Structurally above the staurolite isograd in Fig. 2, roughly 1500 m above the detachment, the dominant assemblage in Carboniferous pelitic rocks is chloritoid + garnet + chlorite or garnet + chlorite + biotite, suggesting temperatures at least 50 K less than those estimated for the kyanite and staurolite zone rocks below. Our limited reconnaissance of the Carboniferous section revealed the presence of numerous normal faults. Although we have not studied these structures in detail, we postulate that they may be responsible for the observed juxtapositioning of metamorphic isograds.

We have recognized four generations of deformational features (D_1 to D_4) at Kang-

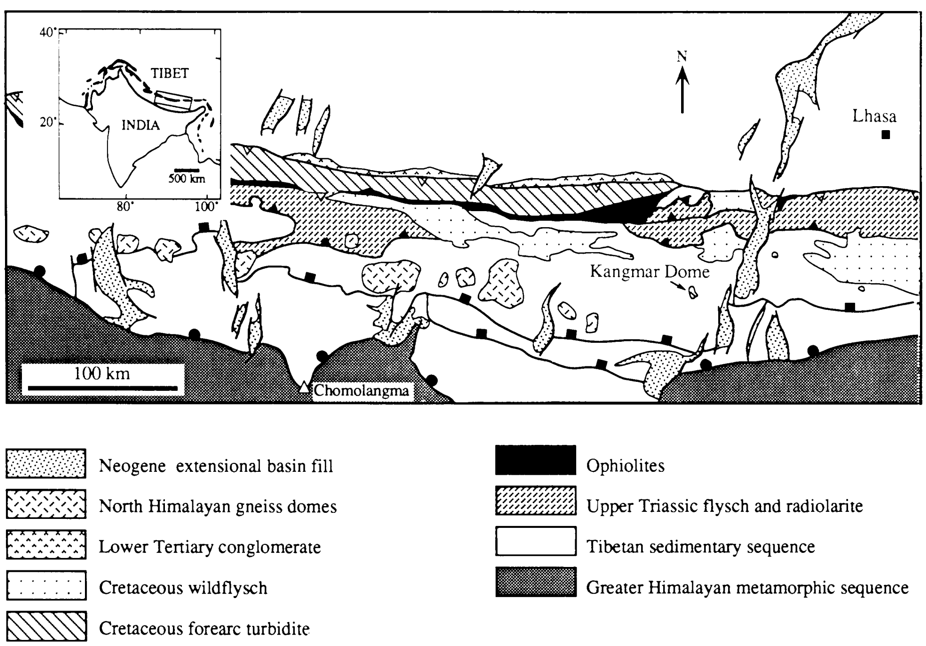

Fig. 1. Generalized tectonic map of southern Tibet after (*8*). Boxed area in inset corresponds to the area of the large map.

mar. The D_1 structures are best developed in the structurally higher parts of the high-grade metamorphic sequence. They include: (i) mesoscopic to macroscopic, tight to isoclinal, west- to northwest-trending folds (F_1); (ii) an associated axial-planar cleavage (S_1); and (iii) an intersection lineation (L_1) that is parallel to F_1 axes. The F_1 folds are commonly overturned to the south or southwest, and F_1 fold trains consistently indicate southward vergence. In low-grade pelitic rocks, inclusion trails (S_i) in chloritoid and garnet porphyroblasts are continuous with S_1 in the matrix; this relation implies that these minerals grew during D_1. Sigmoidal patterns of S_i in many porphyroblasts indicates that the minerals rotated during growth; the sense of rotation is consistent with southward vergence.

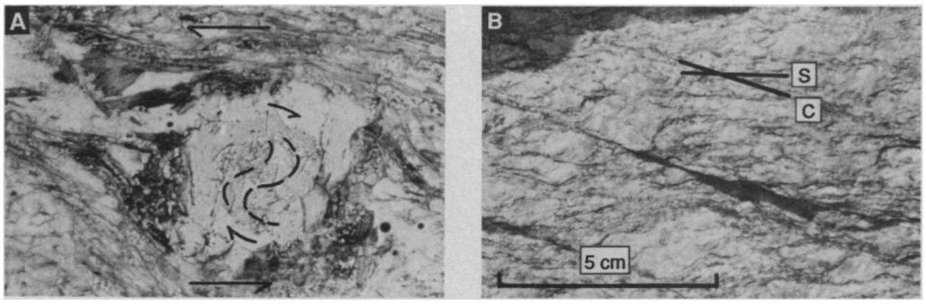

Fig. 4. Fabrics characteristic of the Kangmar dome. (**A**) Photomicrograph (crossed polars) of a garnet porphyroblast from the Carboniferous metasedimentary sequence. Diameter of the porphyroblast is approximately 0.5 cm. Section is cut parallel to L_2 and perpendicular to C_2. North is to the left of the photo. Note that sigmoidal inclusion trails (S_i, formed during D_1, emphasized by heavy dashed lines) indicate southward vergence, while the asymmetry of the pressure shadow around the porphyroblast (a D_2 feature) indicates northward vergence. (**B**) Outcrop of the Kangmar orthogneiss illustrating type I S-C fabrics. Outcrop is oriented parallel to L_2 and perpendicular to C_2; north is to the right. Heavy solid lines represent the intersection of C_2 and S_2 with the plane of the outcrop. A top-to-the-north sense of shear is indicated by the fabrics.

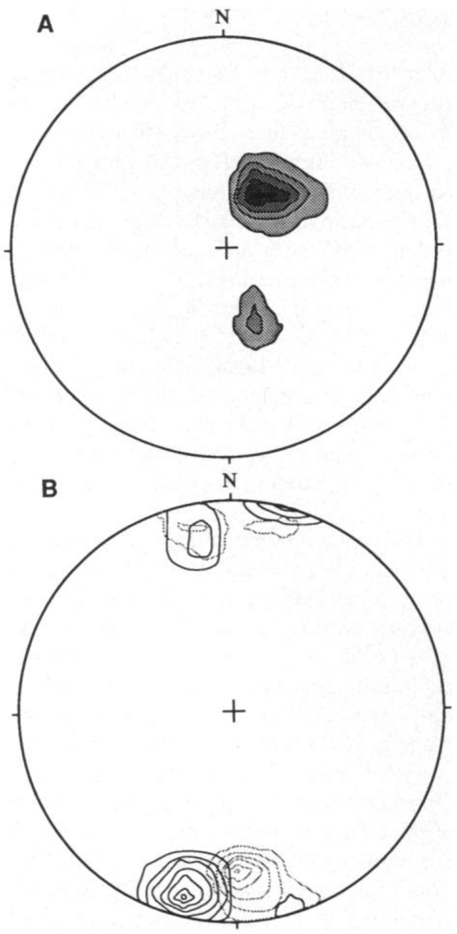

Fig. 3. Lower-hemisphere, equal-area projections of fabric data from the Kangmar dome. Contour intervals are 5% per 1% area. (**A**) Poles to C_2 in both granite orthogneiss and overlying metasedimentary rocks. (**B**) L_2 lineations in granitic orthogneiss (shaded contours) and metasedimentary units (solid contours). Number of measurements is 74 in A and 76 in B.

The D_2 structures, which predominate in the lower part of the metamorphic sequence and throughout the orthogneiss, are related to the early development of the Kangmar detachment. S-C mylonites (*23*) of this age are characterized by well-developed shear planes (C_2), defined by fine-grained, recrystallized micas, and less-pronounced S-planes (S_2), defined by coarse-grained micas and elongate quartz + plagioclase aggregates. The orientation of C_2 varies across the complex, mimicking the overall domical geometry (Fig. 3A). The intensity of C_2 increases markedly in the basal 100 m of the metamorphic sequence. In this zone, S_1 is preserved only locally. Small-scale, intrafolial fold hinges observed in the zone could be transposed F_1 structures or early F_2 folds. Unambiguous F_2 folds are characteristically isoclinal, with axial planes subparallel to C_2 and axes commonly subparallel to a well-developed stretching or mineral lineation (L_2). This lineation is variably defined by the long axes of metamorphic minerals such as kyanite and amphibole, and by elongate quartz + feldspar aggregates. The mean orientation of L_2 is 22° (plunge), N10°W (bearing) on the north side of the dome and 13°, S15°W on the south side (Fig. 3B).

Centimeter- to meter-scale boudinage of more competent lithostratigraphic units and quartz veins is evident near the base of the metamorphic sequence. Boudin necklines lie within C_2 and trend roughly orthogonal to L_2. Many of the observed boudins were asymmetric (*24, 25*), and the long dimensions of the boudins lie within the mylonitic foliation.

Garnet porphyroblasts in the shear zone exhibit textures characteristic of two phases of growth (Fig. 4). Their cores contain rotated inclusion trails similar to S_i in structurally higher rocks. The sense of rotation is consistently top-to-the-south. By analogy with higher units, we assign growth of the garnet cores to M_1 and rotation to D_1. Many overgrowths on these garnets, attributed to a second metamorphic event (M_2), are euhedral, free of inclusions, and have lower Mg/Fe ratios than the cores. Asymmetric pressure shadows, predominantly quartz + plagioclase, have developed around these garnets. The tails of the pressure shadows merge with the mylonitic foliation. Consequently, we interpret M_2 as prekinematic or perhaps early synkinematic with respect to D_2.

Below the Kangmar detachment, the Kangmar orthogneiss displays spectacular S-C mylonitic fabrics (Fig. 5). The C_2 fabric is defined by fine-grained, recrystallized quartz + muscovite + biotite. The S_2 fabric is distinguished by larger mica grains, asymmetric potassium feldspar augen, and the crystallographic preferred orientation of quartz. The orientation of this fabric also follows the overall shape of the dome. The L_2 fabric is defined in C_2 by the elongation of potassium feldspar augen and quartz + feldspar aggregates. The lineation has a mean orientation of 14°, N0°W near Dude and 20°, S4°E on the south side of the dome. We found no evidence for the presence of D_1 structures in the Kangmar orthogneiss.

Several observations lead us to assign a D_2 age to initiation of and principal movement on the Kangmar detachment. First, the intensity of mylonitic fabrics in the metasedimentary rocks increases markedly within 100 m of the detachment. Second, C_2 is everywhere subparallel to the detachment surface. Finally, L_2 lineations above and below the detachment are only slightly discordant, suggesting relatively minor movement along the contact between the orthogneiss and metasedimentary rocks after D_2. We infer that the detachment developed to accommodate D_2 noncoaxial strain during the waning stages of the M_2 thermal event.

Many of the D_2 deformational features at Kangmar have kinematic significance. These include S-C fabrics and stretching lineations, as well as asymmetric augen structures, boudins, and pressure shadows (*26, 27*). In all cases, these indicate that structurally higher rocks moved essentially due northward relative to structurally lower rocks during D_2.

D_3 included the late, low-temperature stages of displacement on the detachment. Localized cataclasis on the detachment was accompanied by the development of slickenslide surfaces, retrograde metamorphism, quartz and calcite veining, and sulfide mineralization. The moderate angular discordance between mylonitic fabrics above and below the detachment (Fig. 3) can be attributed to D_3 movements.

Large-scale doming of the metamorphic sequence occurred during D_4. A cylindrical best-fit girdle to all C surfaces at Kangmar (Fig. 3) corresponds to an axial orientation of 20°, N84°W for the major F_4 structure defining the dome.

In many ways, the structural history we have deduced corroborates the interpretations of earlier workers of an early compressive event (*8, 28*). The recognition of the Kangmar detachment and documentation of northward movement of the hanging wall relative to the footwall indicate, however, that a fundamental change in the direction of material transport from southward during D_1 to northward during D_2 occurred.

The timing of this change is poorly known. No quantitative data constrain the age of M_1 and D_1, although the involvement of paleontologically dated Carboniferous rocks in D_1 structures strongly suggests a Himalayan (Tertiary) age. The minimum age of M_2 is limited by K-Ar and $^{40}Ar/^{39}Ar$ mineral ages. Biotite and muscovite from one high-grade sample yielded $^{40}Ar/^{39}Ar$ plateau ages of 13.5 ± 0.6 and 13.0 ± 0.5 Ma, respectively, and a plateau age of 11.4 ± 0.3 Ma was obtained for a phlogopite from an intercalated marble (*29*). Biotite from a sample of the Kangmar orthogneiss yielded a plateau age of 20.4 ± 0.6 Ma, whereas a muscovite from the same sample produced a saddle-shaped spectrum with a minimum at about 15.5 Ma (*29*). Earlier, Debon and co-workers (*30*) published conventional K-Ar ages ranging from 12.5 to 19 Ma for biotites from the orthogneiss. Maluski and others (*29*) interpreted all of the data as indicative of a single middle Miocene thermal event that included primary growth of the micas in the cover sequence and partial resetting of older micas in the orthogneiss. If this interpretation is correct, we would assign the 13.5 to 13.0 Ma mica ages to the time of cooling through the 575 to 625 K closure-temperature range for these phases (*31*). M_2 temperatures in the lower parts of the metasedimentary sequence exceeded 700 K (*22*). Depending on the cooling rate after the thermal peak, the 13.5 to 13.0 Ma ages may substantially underestimate the age of the M_2 event.

An alternative interpretation of the geochronologic data is possible in light of recognition of the Kangmar detachment. Age discordance across the detachment may indicate that the metasedimentary rocks and orthogneiss had different cooling histories after the M_2 thermal peak but before their juxtaposition during movement on the detachment. In this scenario, M_2 could be substantially older than D_2. We cannot disprove this interpretation, but we do not favor it, given the textural relations between M_2 porphyroblasts and D_2 fabrics in the metasedimentary samples. Although geochronological information from Kangmar is limited, similarities between the available data and age constraints from the Greater Himalayan metamorphic rocks to the south suggest a somewhat more detailed interpretation. Two major phases of prograde metamorphism can be recognized throughout the central sector of the Greater Himalaya: an early, high pressure–intermediate temperature event (M_{1GH}) followed by a later intermediate to low pressure–intermediate temperature event [M_{2GH} (*13, 32*)]. Thermobarometric data for M_{1GH} and M_{2GH} assemblages are strikingly similar to those obtained for M_1 and M_2 assemblages at Kangmar, and it is tempting to correlate the two events. Recent $^{40}Ar/^{39}Ar$ data from the upper part of the Greater Himalayan sequence in a variety of areas suggest that Early to Middle Miocene cooling through the closure temperatures of biotite and muscovite occurred after the M_{2GH} event (*29, 33, 34*). In two of these studies, $^{40}Ar/^{39}Ar$ data for hornblende [with a nominal Ar closure temperature of 775 K (*31*)] imply an age of ~21 Ma for the thermal maximum of M_{2GH} and, by analogy, perhaps for M_2 at Kangmar as well. The age of M_{1GH} is poorly constrained because of the intensity of the M_{2GH} thermal pulse in the central Himalaya, but a few $^{40}Ar/^{39}Ar$ hornblende dates from Garhwal (*35*) and an increasing body of K-Ar and $^{40}Ar/^{39}Ar$ data from the Pakistan Himalaya (*36*) suggest an Eocene age. We speculate that M_1 at Kangmar may have an early Tertiary age as well, but more data are required.

One of the most striking aspects of the Kangmar dome is its similarity to Tertiary metamorphic core complexes of the North American Cordillera (*7, 37*), which developed in an extensional tectonic setting. Like its Cordilleran counterparts, the Kangmar detachment places younger rocks on older and has been conspicuously domed subsequent to its initiation. Northward displacement on the detachment contrasts sharply with the predominant southward transport direction of major thrust structures in the Himalayas (*9, 38*) but is consistent with displacements on the Miocene longitudinal faults that separate the Greater Himalayan sequence from the Tibetan Sedimentary series (*2, 15*). We suggest that the Kangmar metamorphic core complex formed as part of the same Miocene extensional event responsible for the South Tibetan detachment system, and contributed to collapse of the topographic front produced by Eocene to early Miocene compression. If correct, this model implies that extensional features of middle to late Tertiary age are more widespread in southern Tibet than commonly believed.

REFERENCES AND NOTES

1. J. P. Burg and G. M. Chen, *Nature* **311**, 219 (1984).
2. B. C. Burchfiel and L. H. Royden, *Geology* **13**, 679 (1985).
3. K. V. Hodges *et al., Geol. Soc. Am. Abstr. Prog.* **21**, A182 (1989).
4. P. Molnar and P. Tapponnier, *J. Geophys. Res.* **83**, 5361 (1978).
5. B. Dalmayrac and P. Molnar, *Earth Planet Sci. Lett.* **55**, 473 (1981).
6. G. A. Houseman, D. P. McKenzie, P. Molnar, *J. Geophys. Res.* **86**, 6115 (1981).
7. G. H. Davis and P. J. Coney, *Geology* **7**, 120 (1979).
8. J. P. Burg, M. Guiraud, G. M. Chen, G. C. Li, *Earth Planet. Sci. Lett.* **69**, 391 (1984).
9. A. Gansser, *Geology of the Himalayas* (Wiley Interscience, London, 1964).
10. C. F. Chang, Y. S. Pan, H. L. Cheng, X. M. Zhang, *The Geological Structure of the Quinghai-Xizang Plateau* (Science, Beijing, 1982).
11. M. P. Coward *et al.*, in *Tectonic Evolution of the Himalayas and Tibet*, R. M. Shackleton, J. F. Dewey, B. F. Windley, Eds. (The Royal Society, London, 1988), pp. 89–115.
12. M. P. Searle, D. J. W. Cooper, A. J. Rex, *ibid*, pp. 117–149.
13. K. V. Hodges, M. S. Hubbard, D. S. Silverberg, *Philos. Trans. R. Soc. London Ser. A* **326**, 257 (1988).
14. P. LeFort *et al., Tectonophysics* **134**, 39 (1987).
15. J. P. Burg, M. Brunel, D. Gapais, G. M. Chen, G. H. Liu, *J. Struct. Geol.* **6**, 535 (1984).
16. R. Armijo, P. Tapponier, J. Mercier, T. Han, *J. Geophys. Res.* **91**, 13803 (1986).
17. H. H. Hayden, *Mem. Geol. Surv. India* **36**, 122 (1907).
18. Y. S. Zhou, Q. Zhang, H. J. Mei, C. W. Jin, *Magmatism and Metamorphism in Xizang (Tibet)* (Science, Beijing, 1981).
19. Q. Zhang, Y. S. Zhou, G. Z. Li, H. R. Wu, F. G. Wang, *Sci. Geol. Sinica* **2**, 125 (1986).
20. U. Scharer, R. Xu, C. Allegre, *Earth Planet. Sci. Lett.* **77**, 35 (1986).
21. D. Y. Liang and W. P. Wang, *Contrib. Geol. Qinghai-Xizang (Tibet) Plateau* **2**, 226 (1983).
22. K. V. Hodges *et al.*, in preparation.
23. G. S. Lister and A. W. Snoke, *J. Struct. Geol.* **6**, 617 (1984).
24. J. P. Platt and R. L. M. Vissers, *ibid.* **2**, 397 (1980).
25. K. V. Hodges, J. D. Walker, B. P. Wernicke, in *Continental Extensional Tectonics*, M. P. Coward, J. F. Dewey, P. L. Hancock, Eds. (Geological Society of London, Oxford, 1987), pp. 393–408.
26. C. Simpson and S. M. Schmid, *Geol. Soc. Am. Bull.* **94**, 1281 (1983).
27. C. W. Passchier and C. Simpson, *J. Struct. Geol.* **8**, 831 (1986).
28. K. H. He, *Contrib. Geol. Qinghai-Xizang (Tibet)*

Plateau **1**, 250 (1982).
29. H. Maluski, P. Matte, M. Brunel, *Tectonics* 7, 299 (1988).
30. F. Debon, J. L. Zimmerman, G. Liu, C. Jin, R. Xu, *Geol. Rund.* **74**, 229 (1985).
31. I. McDougall and T. M. Harrison, *Geochronology and Thermochronology by the $^{40}Ar/^{39}Ar$ Method* (Oxford Univ. Press, New York, 1988).
32. M. Brunel and J. R. Kienast, *Can. J. Earth Sci.* **23**, 1117 (1986).
33. M. S. Hubbard and T. M. Harrison, *Tectonics* **8**, 865 (1989).
34. K. V. Hodges *et al.*, in preparation.
35. K. V. Hodges and D. S. Silverberg, *Tectonics* 7, 583 (1988).
36. P. J. Treloar *et al.*, *ibid.* **8**, 881 (1989).
37. R. L. Armstrong, *Annu. Rev. Earth Planet. Sci.* **10**, 129 (1982).
38. P. LeFort, *Am. J. Sci.* **275-A**, 1 (1975).

23 August 1990; accepted 31 August 1990

Evolution of a Balanced Sex Ratio by Frequency-Dependent Selection in a Fish

DAVID O. CONOVER AND DAVID A. VAN VOORHEES

Balanced (1 to 1) sex ratios are thought to evolve by a process known as frequency-dependent selection of the minority sex. Five populations of a fish with genetically based variation in temperature-dependent sex determination were maintained for 5 to 6 years in artificial constant-temperature environments that initially caused the sex ratio to be highly skewed. Increases in the proportion of the minority sex occurred in subsequent generations until a balanced sex ratio was established, thus confirming a central premise underlying the theory of sex-ratio evolution.

FISHER WAS THE FIRST TO EXPLAIN why many species tend to invest equally in the production of sons and daughters (*1*). Because every offspring has one mother and father, the contribution of genes from each sex to succeeding generations must be equal. If one sex is less numerous, its per capita contribution is higher and genes that overproduce the minority sex should therefore increase until the primary sex ratio is balanced. Fisher's model hinges on frequency-dependent selection: an evolutionary process where the fitness of a phenotype is dependent on the relative frequency of other phenotypes in the population. Fisher's theory has gained wide acceptance: it potentially accounts for the widespread occurrence of sex-determining mechanisms, such as heterogamety, that ensure the production of 1:1 sex ratios and it is the foundation for virtually all adaptive sex ratio theory (*2*).

Serious doubts have arisen because balanced sex ratios could also simply be a nonadaptive consequence of Mendelian segregation of sex chromosomes (*3*). Moreover, the only direct evidence is the same observation that originally generated the model: the ubiquity of species that have balanced sex ratios in nature (*4*). The dilemma has been that the sex-determining mechanisms of many of these species contain little (if any) genetic variation and, therefore, may not be capable of evolving. Is frequency-dependent selection such a potent evolutionary process that dioecious species capable of producing unbalanced primary sex ratios are rare?

A species ideally suited for directly testing Fisher's theory is the Atlantic silverside, *Menidia menidia*. In this fish, sex is determined by the joint effects of temperature and major sex-determining genes during a specific period of larval development (*5*). The Atlantic silverside is an annual fish that breeds during the spring and summer in bays and estuaries along the east coast of North America. Offspring produced early in the breeding season experience low temperatures that cause most larvae to differentiate into females; high temperatures that prevail during the late breeding season cause most offspring produced then to become male. Previous experiments have conclusively shown that temperature exerts a direct influence on primary sex differentiation rather than causing sex-specific mortality (*5*). The influence of major genes on sex determination is indicated by large nonadditive effects of parentage on the response of sex ratio to temperature within families (*6*). Moreover, the degree of genetic control differs greatly with latitude (*7*). In South Carolina fish, the sex ratio changes by as much as 70% with temperature. The sex ratio of Nova Scotia fish, however, is insensitive to temperature, suggesting complete genetic control. Fish from New York show an intermediate sex ratio response to temperature.

In nature, the normal pattern of seasonal change in temperature usually results in a sex ratio close to 0.5 (*5*). When progeny from a natural population are transferred to a constant-temperature environment, however, the resulting sex ratio can be highly skewed. We established five separate laboratory populations of silversides that constantly experienced either a high or low temperature environment during development each generation. Two populations were started in 1984 by randomly subdividing a common stock of several thousand newly hatched larvae that were collected as embryos from South Carolina (*8*). One such population was reared during the temperature-sensitive period at 28°C (SC-H) and the other at 17°C (SC-L). This produced sex ratios (F/F+M) that were skewed in the initial generation toward opposite extremes: 0.18 in SC-H, 0.70 in SC-L. Fish in each line were reared to maturity and allowed to spawn en masse in laboratory tanks (*9*). Their progeny were reared at the same high or low temperature during the sensitive period of larval development as were their parents. After the sensitive period, juvenile fish were subsampled to estimate the sex ratio (*10*) and about 100 remaining fish were reared to sexual maturity (*11*). Subsequent generations were treated to a like manner. Two other populations were established in 1985 with field-collected New York embryos and maintained as above, but in these lines the initial sex ratios at 28°C (NY-H) and 17°C (NY-L) were 0.05 and 0.29, respectively. The fifth population was founded in 1985 with embryos from Nova Scotia, where the sex ratio is close to 0.5 at all temperatures. This laboratory population (NS-H) was reared at 28°C each generation (*12*).

There are five possible general outcomes to this experiment. (i) No changes in sex ratio among generations. (ii) Random changes in sex ratio as might be caused by the effects of genetic drift. (iii) Shifts in sex ratio depending directly on thermal environment (that is, all high temperature lines change in a like manner, all low lines in another). (iv) Increases in the proportion of the majority sex, perhaps leading to the loss of one sex. (v) Increases in the proportion of the minority sex, with convergence of the sex ratio to 0.5. Only alternative (v) would support Fisher's theory. Note that we can distinguish between alternatives (iii) and (v) because the SC-L line begins with a female excess while the NY-L line begins with a male excess. Moreover, the NS-H population serves as a control because its sex ratio starts at 0.5 and is therefore not expected to change.

Changes in sex ratio closely followed the predictions of Fisher's theory. Increases in the minority sex occurred in each of the four populations that started with skewed sex

Marine Sciences Research Center, State University of New York, Stony Brook, NY 11794–5000.